Plasma Science and Technology

PAPER

Characterization of an ionic liquid electrospray thruster with a porous ceramic emitter

Plasma Sci. Technol. **22** (2020) 094009 (9pp) https://doi.org/10.1088/2058-6272/ab9528

Characterization of an ionic liquid electrospray thruster with a porous ceramic emitter

Chong CHEN (陈冲), Maolin CHEN (陈茂林) and Haohao ZHOU (周浩浩)

Combustion, Internal Flow and Thermal-Structure Laboratory, Northwestern Polytechnical University, Xi'an 710072, People's Republic of China

E-mail: chenmaolin@nwpu.edu.cn

Received 2 January 2020, revised 19 May 2020
Accepted for publication 20 May 2020
Published 29 July 2020

Abstract

An ionic liquid (IL) electrospray thruster was developed for application in micro-nano satellites or gravitational wave detectors. The thruster employed a porous ceramic emitter with seven emitter strips located on its emission surface. Without any liquid-supply device, IL was delivered through porous media to emitter strips via capillary effect. Multiple emission sites then formed at the tip of each strip. A charged beam of up to 350 μA (with a current density of 540 μA cm^{-2}) was stably produced in the negative mode. However, in the positive mode, a corona was observed which could prevent the thruster from emitting larger current. A time-of-flight mass spectrometer with significantly improved signal-to-noise ratio was built, which was used to obtain the mass distribution of the beam of the thruster. A retarding potential analysis was also performed. The test results showed that the thruster worked in the pure-ion regime, and delivered a maximum thrust of 67.1 μN with specific impulses of 3952 s and 3117 s in the positive and negative modes, respectively.

Keywords: electrospray thruster, time-of-flight (TOF), retarding potential analysis (RPA)

(Some figures may appear in colour only in the online journal)

1. Introduction

The Electrospray thruster [1] can be used for space missions such as micro-nano satellite orbit maintenance or maneuvering, formation flight, and gravitational-wave detection. This thruster produces thrust by emitting ions and droplets from a charged surface (i.e. the phenomenon of electrospray [2]). When a liquid is placed in a strong electric field, its surface deforms because of electrostatic force. If the field strength exceeds a threshold (i.e. the onset voltage of a Taylor cone), the liquid surface will be stretched as a cone, which is called a Taylor cone [3]. Although the Taylor cone appears stable, it is not static. At its tip, either a droplet beam is generated as a result of the charge relaxation [4] (i.e. the pure droplet emission) or an ion plume is generated via the field evaporation [5] (i.e. the pure ion emission), or both the phenomena occur [6] (i.e. the ion-droplet mixed emission) to maintain a dynamic equilibrium of the whole process. As the thrust produced by a single Taylor cone is very small (generally about 0.1 μN), a Taylor cone array is usually used to improve the thrust of the electrospray thruster. To reduce the onset voltage [7], the Taylor cone array is generally produced on an emitter, which is typically an electrode with several tiny bulges on its surface.

Compared with plasma propulsion, there is no need to generate plasma via a gas discharge. Thus, the electrospray thruster avoids the decreased efficiency caused by the decreased thruster size. Also, the small size and low power characteristics enable the thruster to fully meet the requirements of micro-nano satellites. Additionally, the propellant used by an electrospray thruster (e.g. ionic liquids (ILs)) has a moderate surface tension. This leads to a lower operating voltage compared to the field emission electric propulsion [8, 9]. Also, ILs are liquid at room temperature, and hence, they do not require heating. Compared with colloidal thrusters [10], an increase in ionic components in the thruster's beam greatly increases its specific impulse.

There are three main types of IL electrospray thrusters: internally fed, externally wetted, and porous. Internally fed thrusters use capillary array as emitter and typically require a large liquid feed system to deliver the propellant to the capillary port. It is difficult to raise the flow resistance of the capillary to a sufficiently large value, which is necessary for improving the emission uniformity of the emitter array [11]. Although Krpoun [12] and Lenguito [11] filled the capillaries with little beads and Dandavino [13] adopted deep reactive ion etching to lengthen the emitters, the number of ignited emitter capillaries was only around one hundred, and the emission current reached only tens of μA. Recently, Inoue [14] used an interesting method that successfully reduced the aperture of the capillaries to the sub-μm scale. This resulted in an emitter array density as high as 4 million cm^{-2} and an emission current density as high as about 1 mA cm^{-2}. However, the structure seems to be vulnerable to leakage of ILs.

In an externally wetted thruster, propellant is brought to emission by wetting the surface of the emitter. As the supply path is limited in a 2D surface, it is very unstable. Methods such as deposition of black silicon [15] or carbon nanotubes [16] on the surface are necessary for improving the wettability of the surface. Using this second approach, the emission current reached an attractive 1.35 mA on a 1 cm^2 emission surface with 1900 emitter tips. However, the problem of supply was not fully addressed. During the reported test, IL was dripped onto the surface of the emitter. This approach can only sustain short-time emission.

A porous electrospray thruster does not require any liquid feeding device. The IL can be adsorbed from the reservoir via the capillary effect to the tip of the emitter. Also, according to the consumption amount caused by the electrospray, the amount of feed will be automatically adjusted under the action of an electric field. Recently, this kind of thruster has been extensively studied. The most well-known scalable ion electrospray propulsion system (S-iEPS) integrated 480 porous glass emitter tips on a 1 cm^2 emission surface, and the whole thruster had a volume scale of 1 cm^3 [17, 18]. It could achieve a specific impulse of $\sim$1000 s with an approximate thrust density of 12 μN cm^{-2}. Liu combined wire electrical discharge machining with electrochemical etching to solve the problem of blockage of pores close to the surface when porous metals are used to prepare emitters [19]. Ma produced a current of 100 μA with only one emitter tip (5 mm tall) [20].

Previous studies employed a form of emitter array to improve thrust density [13, 14, 16]. This form of emitter generally needed complex and expensive manufacturing techniques to increase the array density. Also, locations of emission sites were strictly limited to emitter tips. If the emitter array was not well designed (or manufactured), the number of ignited emitter tips would be reduced dramatically. Courtney [21] adopted a more convenient emitter form. Nine strips were processed via traditional CNC machining on the surface of a porous glass. Multiple emission sites formed at the tip of each emitter strip if local condition parameters, such as field strength and amount of liquid, were suitable. According to tests, this thruster had the same level of performance as S-iEPS.

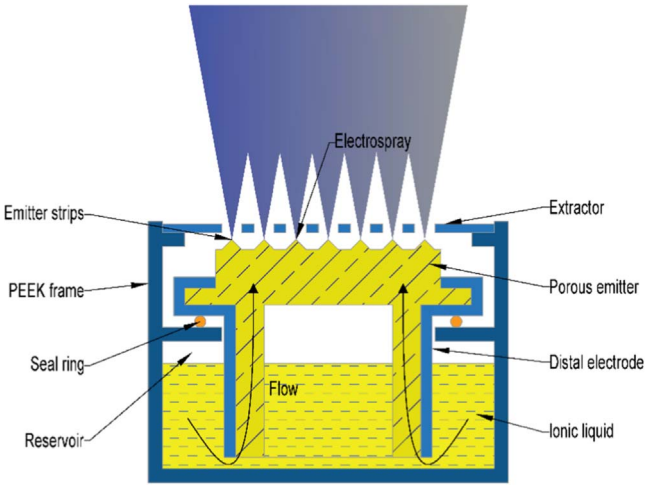

Figure 1. Structure of the electrospray thruster.

In this study, an IL electrospray thruster with a porous ceramic emitter was developed. The form of emitter strips was adapted. To overcome the incompatibility between machining and hard materials, such as borosilicate glass or ceramic, a sintering process was used to prepare the porous ceramic emitter. Section 2 gives a description of the thruster. In the design, several problems were considered, such as insulation failure caused by a leakage of IL, decay of the IL supplied by a porous reservoir, and electric field non-uniformity between the ends and the middle of the emitter strips. To investigate the thruster's performance, emission current measurement, retarding potential analysis (RPA), and time-of-flight (TOF) diagnosis were performed. Section 3 describes all the test methods. Section 4 gives test results and a discussion.

2. Description of the thruster

As shown in figure 1, the thruster investigated in this study mainly consisted of an emitter, extractor, and reservoir. The emitter was made of a porous ceramic material with a pore size between 1 and 10 μm. There were seven emitter strips protruding from the emission surface, with dimensions of 8 mm $\times$ 8 mm. The emitter strips, which had a triangular cross-section, were 300 μm in height with an apex radius of approximately 20 μm. The whole porous emitter was 2.5 cm high so that its bottom could extend into the reservoir, which was filled with ILs. The extractor was about 500 μm away from the emitter and had a thickness of 1 mm and 7 slots. The slots were 600 μm wide. The extractor and emitter were aligned using a microscope. All the components were installed on a polyaryletheretherketone (PEEK) frame. The size of this thruster was 30 mm $\times$ 30 mm $\times$ 27 mm. Figure 2 shows photographs of the thruster.

In previous studies [20, 21], a porous borosilicate disc was attached to the bottom of the emitter and it was used as the reservoir. As the IL in the porous reservoir was consumed by electrospray, the charged beam emitted by the thruster continued to decrease [22]. To avoid degradation of thruster

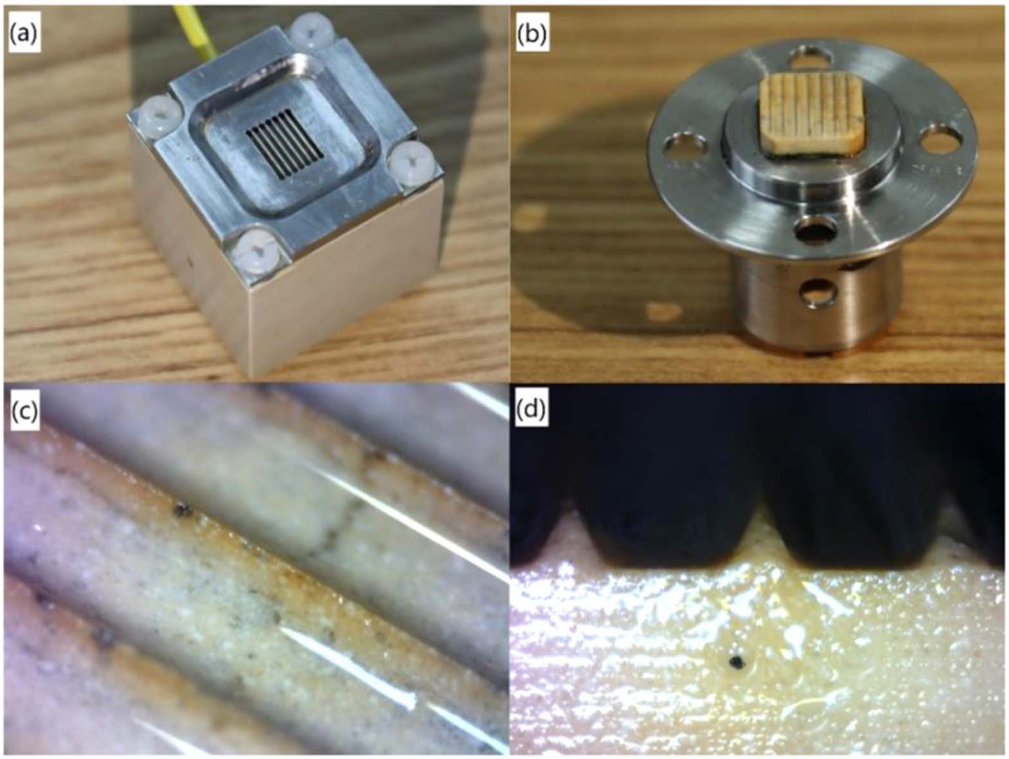

Figure 2. The electrospray thruster: (a) the thruster, (b) the porous emitter embedded in a distal electrode, and (c), (d) photomicrographs of the emitter strips.

performance over time, a tank was used in this study, as shown in figure 1. The bottom of the porous emitter was immersed in the IL stored in the tank so that the emitter was always in a saturated state, i.e. the volume of IL adsorbed by the emitter was basically constant until the IL in the tank ran out.

Obviously, ends of an emitter strip have a larger curvature than the middle, which means that there is a stronger electric field. Therefore, after a voltage is applied between the emitter and the extractor, Taylor cones will first form at ends of the emitter strip. As the voltage increases, these Taylor cones will become unstable first, which would cause the emitted current to stop increasing with voltage. Thus, in this study, enlarged holes were opened in ends of the extractor-slots to reduce the local electric field intensity. The same structure was also adopted in [23].

Application of ILs in a compact electrospray thruster usually causes great insulation problems. When the thruster is working, the liquid is at a high potential of thousands of volts. Any accidental contact with low-potential parts may cause an electric leakage or even a short circuit. The risk is very high because of the fluidity of the liquid. In the design of this thruster, the distance between the emission surface and the extractor was much smaller than the distance between the other high-voltage (HV) parts and the extractor to prevent an accidental discharge. Additionally, a groove was left between the PEEK frame and the distal electrode in contact with the IL, which prevented the IL from climbing onto the frame. At the same time, the extractor was suspended and supported above the emitter by four corner gaskets, and it reduced the contact area between the extractor and the frame.

For the same reason, the tank was sealed using a seal ring. However, the residual pressure in the tank squeezed the IL out of the porous emitter, which resulted in a short circuit between the emitter and the extractor. Thus, a hole (referred to as an air-release-hole) was then opened on the side of the reservoir to balance the internal and the external pressure. However, as discussed in section 4.1, when the voltage between the emitter and the extractor was large, a positive corona formed around the hole, preventing the thruster from working steadily.

3. Experimental apparatus and methods

All experiments were performed in a vacuum chamber with size of Ø0.5 m × 1 m. Using a mechanical pump (10 L s^{-1}, VP-2020, VALUE, Wenling, China) and molecular pump (600 L s^{-1}, JTFB-600, Beijing, China), the minimum pressure that this chamber can achieve was about 1×10^{-3} Pa. All the experiments were performed under this pressure unless otherwise mentioned. 1-Ethyl-3-methylimidazolium-tetrafluoroborate (EMI-BF_4, Aiwei, Suzhou, China) was used as the propellant. After the propellant was loaded, the thruster was placed in the vacuum chamber for a period of time to release the gas adsorbed by the IL and the porous medium. To avoid the effects of gravity, the thruster was placed horizontally with the emission surface facing up.

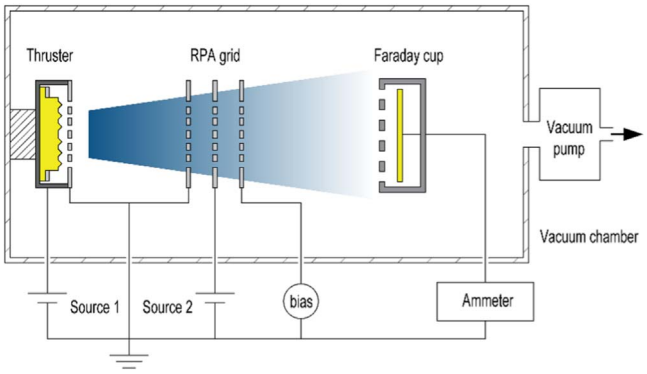

Figure 3. RPA experimental system.

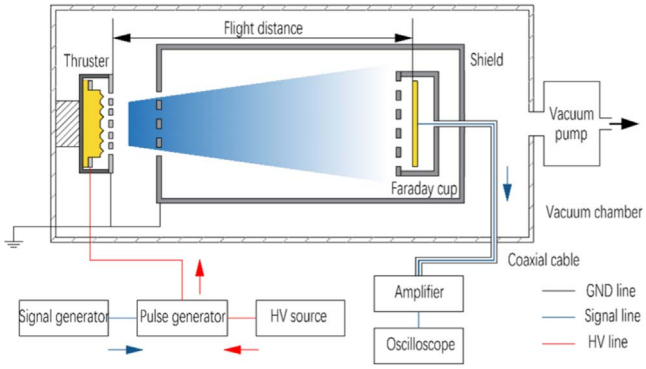

Figure 4. TOF mass spectrometry system.

3.1. I–V characteristics

A two-channel (one positive and one negative) DC HV electric source (HB-S502-10AC, Hengbo, Ningbo, China) with a maximum output voltage of 10 000 V was used to provide the thruster voltage. During the experiment, the extractor and the ground terminal of the source were grounded, and the emitter was connected to the positive or negative terminals of the source. The built-in ammeter of the HV source was used to directly read the emitter current (I_{em}), and an ammeter connected in series was used to measure the extractor current (I_{ex}).

3.2. RPA measurements

The energy distribution of the beam was measured using an RPA system, as shown in figure 3. The thruster beam passed through three semitransparent grids and was then received by a Faraday cup. The beam current was finally measured by an ammeter connected to the Faraday cup. The first grid was grounded. A potential of –20 V was applied to the last grid to suppress secondary electron backflow. The middle grid was the RPA grid. During the experiment, the potential of the RPA grid was gradually increased/decreased from 0 V. If an ion had a kinetic energy equal to the retarding potential (in eV), then that ion was stopped and was not collected by the Faraday cup. Thus, the collected current was measured as a function of the retarding potential to yield the energy distribution of the beam.

3.3. TOF measurements

TOF measurements can usually be used to determine the beam composition and the performance of the electrospray thruster. After charged particles are accelerated by the electric field between the emitter and extractor, charged particles with different charge-to-mass ratios travel at different speeds:

$$v_i = \sqrt{\frac{2q_i V_0}{m_i}} \tag{1}$$

and take different times to move a distance (i.e. the flight distance):

$$t_i = \frac{L}{v_i} = L\sqrt{\frac{m_i}{2q_i V_0}}, \tag{2}$$

where m_i and q_i respectively denote the mass and charge of a charged particle, V_0 denotes the voltage between the emitter and the extractor, and L denotes the flight distance. This is the basis for TOF mass spectrometry, through which charge-to-mass ratios of charged particles can be determined from their flight times. When the thruster works steadily, charged particles reach the detection device. Then, a steady signal is acquired by a signal acquisition device connected to the detection device. At this time, if the beam is intercepted at a position in front of the detection device, only the beam behind the position can reach the detection device. After a while, the fastest particle reach the detection device and disappear from the signal. A slower particle then reach the detection device and disappear. When all the particles arrive at the detection device, the beam signal returns to zero. Hence, an $I(t)$ curve (where I denotes current, and t denotes time) is acquired, and the mass distribution of the beam can be obtained according to formula (2).

There are two ways to intercept the beam: (1) periodically gating the beam while maintaining emitting particles [24] or (2) periodically setting the voltage difference between the extractor and the emitter to zero. In method (1), a triple grid (i.e. an electrostatic gate) is used, which can significantly reduce the intensity of the beam signal. Coupled with the effect of beam divergence, the effective signal obtained is often less than 10% of the emitted current. Also, multiple grids can introduce a considerable amount of oscillation noise. Thus, method (2) was adopted.

The experimental system is shown in figure 4. To improve the switching speed, the power of the thruster was provided by an HV pulse generator (PVX-4140, DEI Scientific, Fort Collins, CO, USA) that had a rise/fall time less than 25 ns. The control signal of the pulse generator was provided by a signal generator (VC2000, VICTOR, Shenzhen, China) that generated a square wave of 0.5 Hz. The flight distance was 37 cm, and the beam detection device was a Faraday cup. As the signal detected could be as small as a few hundred nA, an amplifier (DHPCA-100, FEMTO, Berlin, Germany) was used with its magnification set to 10^6 V A^{-1} (with a bandwidth of 1.8 MHz). An oscilloscope (UTD2102CEX, UNI-T, Dongguan, China) with a bandwidth of 100 MHz was used to record the $I(t)$ signal.

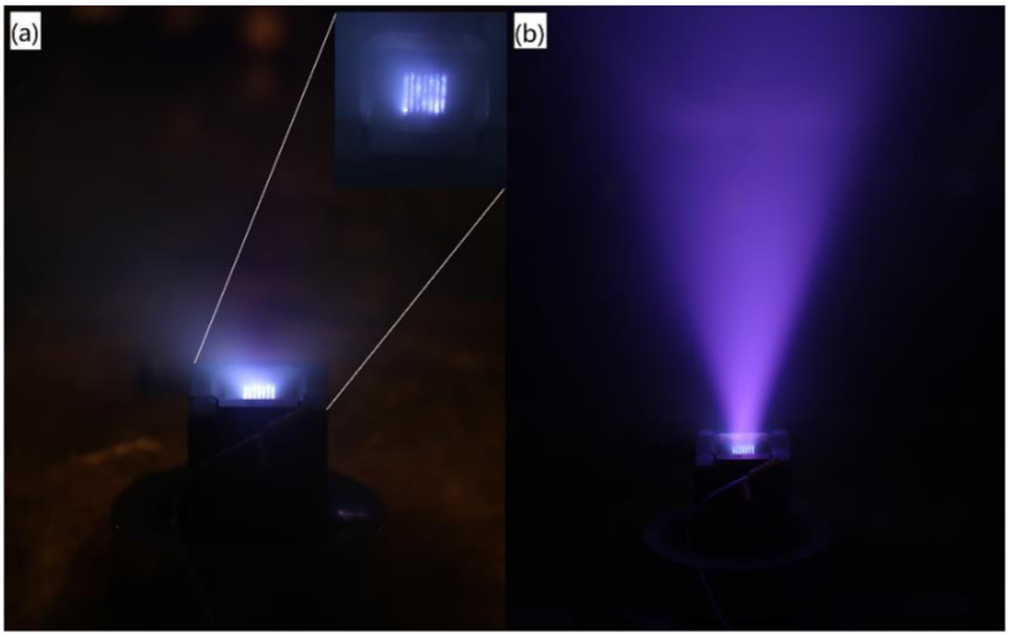

Figure 5. Ignition photos of the thruster. (a) Under 1×10^{-3} Pa, (b) under 0.1 Pa.

The success of TOF mass spectrometry depends on whether noises in the signal can be reduced. To this end, the following measures were taken: (1) the signal detection device was doubly shielded, (2) a coaxial line (without electrical contact with the vacuum chamber) was used to transmit the $I(t)$ signal, and (3) a low-pass filter (i.e. a resistor) was applied in series between the amplifier and the thruster [6].

4. Results and discussion

Before presenting test results, a display of the working state of the thruster is given. Figure 5(a) is an ignition photograph of the thruster under about 1×10^{-3} Pa, and its top view is shown in the upper right inset. Almost all the strips were lit, and the brightness was relatively uniform. In figure 5(b), the pressure of the vacuum chamber was intentionally increased to about 0.1 Pa by turning off the molecular pump of the vacuum chamber, in order to increase the collision frequency of the charged particles. Thus, the light generated by metastable ions provided the spatial distribution information of the beam. The beam divergence angle was less than 50°.

It is generally thought that electrospray does not glow like a gas discharge because it is just a process of a liquid jet breaking up. However, this is only the case for the pure droplet regime. For a process that involves ionization, glowing is natural. When an electrospray is in the pure ion regime or mixed regime, ion evaporation in the surface of a conducting liquid is also an ionization process. Hence, even in a vacuum, a faint light on the surface of the emitter is often seen.

4.1. I–V characteristics

Figure 6 shows the *I–V* characteristics of the thruster. The onset voltage was about 2 kV. With an increase in the voltage, I_{em} first increased exponentially, and then increased linearly. In the negative emission mode, I_{em} was as high as 350 μA at a voltage of 3600 V, and the emitted current was relatively stable. With a further increase in the voltage, the emission current reached 700 μA, but became very unstable. The beam current of positive polarity was slightly higher than that of negative polarity in the same voltage. However, in the positive mode, emission instability appeared when the emitted current exceeded 100 μA, which was far less than the current in the negative mode. To investigate the extraction efficiency of the extractor, I_{ex} was also measured. As shown in the figure, almost one third of the beam current was intercepted by the extractor.

In this experiment, the pressure of the vacuum chamber was about 10^{-3} Pa, which was much lower than the pressure needed for gas discharge. Nevertheless, a corona was observed outside the housing of the thruster when it was in the positive mode. As displayed in figure 7, a fingerprint outside the thruster glowed faintly. The pressure around the thruster was probably higher than the value displayed on by the vacuum gauge. The fingerprint was likely due to a small amount of IL accidentally attached to the housing of the thruster during installation. These liquids then joined with the liquid in the reservoir, which was at a high potential, through the air-release-hole. Therefore, the liquids outside the housing became an electrode of a corona discharge. As the voltage of

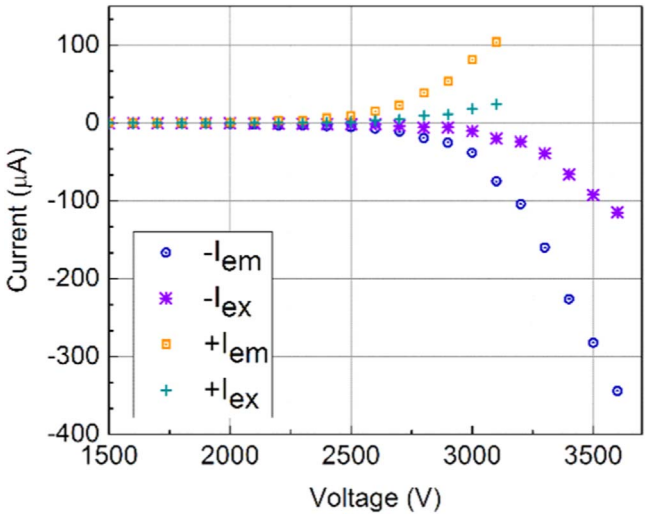

Figure 6. *I–V* characteristics of the thruster.

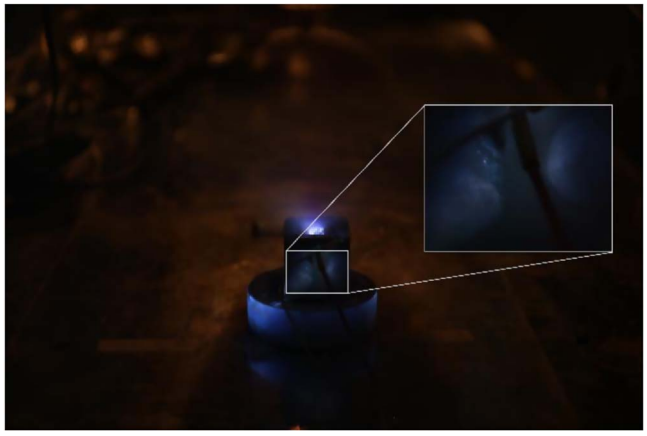

Figure 7. Positive corona outside the thruster.

the thruster increased, the intensity of the corona increased. Hence, electric leakage also increased, which directly caused instability of the electrospray. It is known that it is more difficult to form a negative corona than a positive corona [25]. Hence, the thruster was much less affected under a negative voltage than under a positive voltage.

The large interception rate of the extractor can be attributed to the large alignment-error between the extractor and the emitter and to the large thickness of the extractor.

4.2. RPA measurements

Figure 8 shows the RPA curves in both the positive and negative emission modes. The corresponding energy distribution of each mode is also given in the upper right corner of each panel. The voltage differences (V_0) between the emitter and the extractor were 2.9 kV and 3.4 kV in the positive and negative modes, respectively. Two peaks were present in the positive energy distribution: the first was at $\sim 0.35V_0$, and the second was at $\sim V_0$. Also, there was little distribution elsewhere. In the negative mode, the energy distribution spread throughout the interval [0, V_0]. Although the distribution peak was still present at $\sim 0.3V_0$ and $\sim V_0$, it was not as significant as in the positive mode.

If all the particles have a kinetic energy equal to the emitter-extractor-potential (in eV), then the RPA curve will have a sharp step only in V_0. Sloped transitions between discrete collected current drops indicate a population of particles that have a distribution of kinetic energy. There are two main reasons for this distribution: (1) ion extraction and (2) solvated ion fragmentation. As little energy was used in the desorption of ions from the liquid surface [26], only the second case is discussed.

Electrospray of IL typically produces single ions and ion clusters (i.e. solvated ions). Single ions (e.g. EMI^+ or BF_4^- in this study) are referred to as monomers. A dimer (e.g. [EMI-BF_4] EMI^+ or [EMI-BF_4] BF_4^- in this study) is a single ion attached to a single cation–anion pair. A trimer (e.g. [EMI-BF_4]$_2$ EMI^+ or [EMI-BF_4]$_2$ BF_4^- in this study) is a single ion attached to two neutral species, and so on. Table 1 gives the mass of several monovalent ions, which are most likely to occur when EMI-BF_4 is used for the electrospray.

Ion clusters are metastable and can break up during flight; this phenomenon is referred to as fragmentation [27]. Fragmentation features on the RPA curve depend on whether solvated ions break up in the field-free space or in the acceleration region. If a solvated ion breaks up in the field-free space, it is no longer accelerated, and it has a kinetic energy of:

$$K_{\mathrm{bi}} = \frac{m_{\mathrm{i}}}{m_{\mathrm{pi}}} q_{\mathrm{i}} V_0, \tag{3}$$

where K_{bi} is the kinetic energy of the broken ion, m_{i} is the mass of the broken ion, m_{pi} is the mass of the parent ion, q_{i} is the charge of the broken ion, and V_0 is the accelerating potential. For a given accelerating potential, the kinetic energy is a constant value that only depends on the masses of the parent and broken ions. Fragmentation in the field-free space appears as sharp steps in the current because the energy is the same for all the broken ions of a given species that are created in the field-free space.

After [EMI-BF_4] EMI^+ was split into EMI^+ and [EMI-BF_4] in the field-free space (denoted as [EMI-BF_4] $EMI^+ \rightarrow EMI^+$), the energy of EMI^+ was $0.36V_0$, according to equation (3). This is consistent with the first step (at $\sim 0.35V_0$) of the RPA curve in figure 8(a). Similarly, the first step (at $\sim 0.30V_0$) of the RPA curve in figure 8(b) indicates the event of [EMI-BF_4] $BF_4^- \rightarrow BF_4^-$ in field-free space.

When fragmentation occurs in the acceleration region, the broken ion continues to be accelerated, and its final kinetic energy is:

$$K_{\mathrm{bi}} = q_{\mathrm{i}}\left(\left(\frac{m_{\mathrm{i}}}{m_{\mathrm{pi}}} - 1\right)V_{\mathrm{B}} + V_0\right), \tag{4}$$

where V_{B} is the local value of the potential at which the parent ion breaks up. Fragmentation in the acceleration region produces broken ions with a spread in kinetic energies, and therefore, the RPA curves will have sloped features. By measuring the heights of the steps and slopes, the current fraction due to each type of fragmentation can be determined.

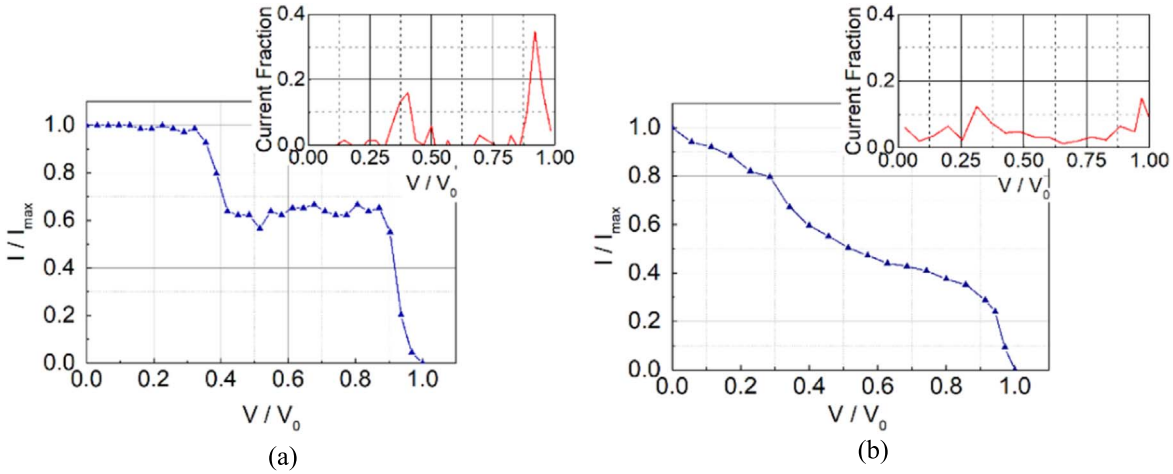

Figure 8. RPA curves of the thruster beam: (a) positive mode and (b) negative mode.

Table 1. Mass of ions that may occur in an EMI-BF_4 electrospray beam.

	$[EMI\text{-}BF_4]_n\ EMI^+$			$[EMI\text{-}BF_4]_n\ BF_4^-$		
	$n=0$	$n=1$	$n=2$	$n=0$	$n=1$	$n=2$
Mass (Da)	111.2	309.1	507.1	86.8	284.8	482.8

If the event $[EMI\text{-}BF_4]\ EMI^+ \rightarrow EMI^+$ occurs in the acceleration region, the energy of EMI^+ will be distributed in the interval $[0.36V_0, V_0]$. If the event $[EMI\text{-}BF_4]\ BF_4^- \rightarrow BF_4^-$ happens in the acceleration region, the energy of BF_4^- will be distributed in the interval $[0.30V_0, V_0]$. The current fraction for each particle is given in table 2.

4.3. TOF measurements

The original signal acquired by the TOF diagnostic system is shown in figure 9. A total of 16 cases were diagnosed. Even when the acquired signal was as weak as 100 nA and the flight distance was limited to 37 cm by the vacuum chamber, the diagnostic system could still distinguish the falling/rising edge of the signal.

For convenience, the horizontal axis of the above graph was converted to mass using equation (5):

$$m_\mathrm{i} = \frac{2 \times 10^3 q_\mathrm{i} V_0 N_\mathrm{A}}{L^2} t_\mathrm{i}^2, \tag{5}$$

where N_A is Avogadro's number, and q_i, the charge of ion, equals to the elementary charge. Also, a simple low-pass filter was used to reduce the small high-frequency noise in the TOF curve. The final results are shown in figure 10.

There are two obvious steps in both the positive and negative modes, which correspond to the monomers (EMI^+ or BF_4^-) and dimers ($[EMI\text{-}BF_4]\ EMI^+$ or $[EMI\text{-}BF_4]\ BF_4^-$), respectively. In all the positive cases, n (i.e. the number of cation–anion pairs) did not exceed 2. In the negative mode, solvated ions with a slightly larger n appeared. Large (mass) droplets were not present in the beam. Thus, the thruster worked in the pure ion regime.

Proportions of various ions in the beam for each case were counted. According to the results, the voltage has no significant effect on composition. Hence, for brevity, average values of all the cases are given in table 3.

Based on the TOF curve, the thruster performance (in terms of thrust and specific impulse) can be determined using equations (6) and (7) [28]:

$$T = \frac{2V_0 I_\mathrm{b}}{L} \int_0^\infty t \left| \frac{\mathrm{d}\bar{I}}{\mathrm{d}t} \right| \mathrm{d}t \tag{6}$$

$$I_\mathrm{sp} = \frac{L \int_0^\infty t \left| \frac{\mathrm{d}\bar{I}}{\mathrm{d}t} \right| \mathrm{d}t}{g \int_0^\infty t^2 \left| \frac{\mathrm{d}\bar{I}}{\mathrm{d}t} \right| \mathrm{d}t}, \tag{7}$$

where T denotes thrust, I_sp denotes specific impulse, V_0 denotes the emitter-extractor voltage, I_b denotes the beam current, L denotes the flight distance, $\bar{I}$ denotes the normalized current, t denotes time, and g is the acceleration of gravity.

If the influence of voltage on the shape of the TOF curve is not considered, two average values of the eight cases in each mode can be computed to reduce the individual error in the numerical integration process:

$$\Gamma_\mathrm{ave} = \frac{1}{8} \sum_{i=1}^{8} \int_0^\infty t \left| \frac{\mathrm{d}\bar{I}}{\mathrm{d}t} \right| \mathrm{d}t \tag{8}$$

$$\Lambda_\mathrm{ave} = \frac{1}{8} \sum_{i=1}^{8} \frac{\int_0^\infty t \left| \frac{\mathrm{d}\bar{I}}{\mathrm{d}t} \right| \mathrm{d}t}{\int_0^\infty t^2 \left| \frac{\mathrm{d}\bar{I}}{\mathrm{d}t} \right| \mathrm{d}t}. \tag{9}$$

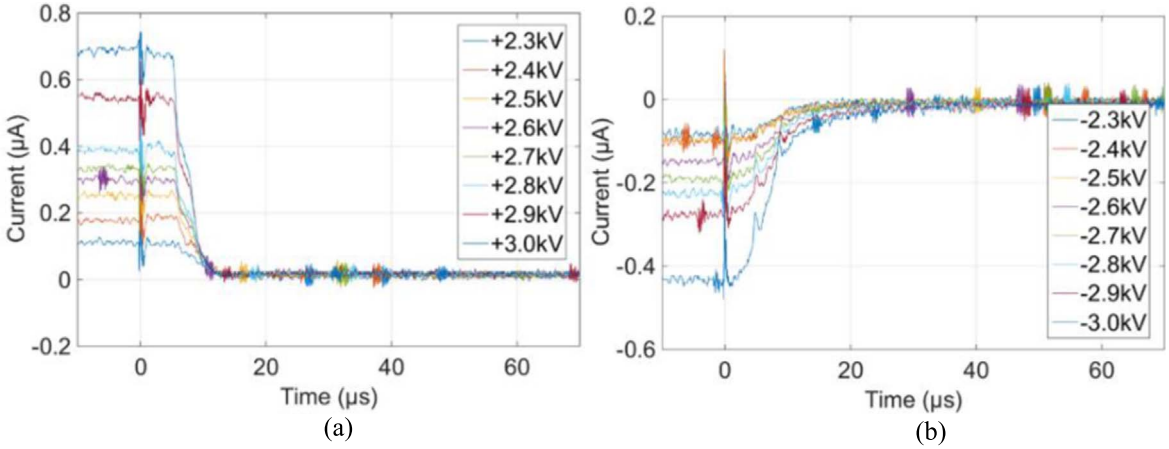

Figure 9. Original signals acquired by the TOF mass spectrometry system: (a) positive mode, and (b) negative mode.

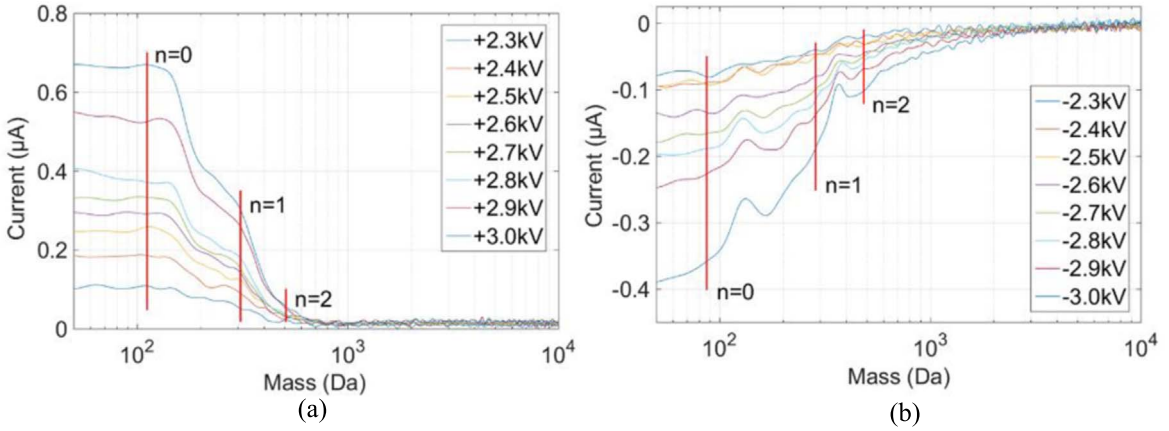

Figure 10. Mass distribution of the thruster beam: (a) positive mode and (b) negative mode.

Table 2. Current fraction due to each type of fragmentation.

	[EMI-BF_4] $EMI^+ \rightarrow EMI^+$			[EMI-BF_4] $BF_4^- \rightarrow BF_4^-$		
Ions	Field-free	Acceleration	Unbroken	Field-free	Acceleration	Unbroken
Fraction	0.4	0	0.6	0.5	0.2	0.3

Table 3. Average proportion of ions in the thruster beam.

	$[EMI\text{-}BF_4]_n$ EMI^+			$[EMI\text{-}BF_4]_n$ BF_4^-		
	$n = 0$	$n = 1$	$n > 1$	$n = 0$	$n = 1$	$n > 1$
Proportion (%)	52.2	35.5	12.3	43.6	25.4	30.9

The thrusts in each case and the specific impulses can then be calculated according to the following equations:

$$T_i = \frac{2V_{0i}I_{bi}}{L}\Gamma_{\text{ave}} \tag{10}$$

$$I_{\text{sp}} = \frac{L}{g}\Lambda_{\text{ave}}, \tag{11}$$

where i denotes the order number of a case.

According to equations (8)–(10), the thruster has specific impulses of 3952 and 3117 s in the positive and negative modes, respectively. The maximum thrusts are 14.5 and 67.1 μN in the positive and negative modes, respectively.

5. Conclusion

An IL electrospray thruster with a porous ceramic emitter was developed. The emitter had seven emitter strips located on the emission surface, which had an area of 0.64 cm^2. In the design, several problems were considered, such as insulation

failure caused by a leakage of IL, decay of flow rate of IL over time in a porous media, and nonuniformity of electric field between ends and the middle of the emitter strip. Both the emitter current (I_{em}) and extractor current (I_{ex}) were measured. I_{em} was as high as 350 μA at a voltage of +3600 V. A corona was observed in the positive mode, which could prevent the thruster from emitting larger current. Furthermore, a RPA was also performed. According to the results, the energy distribution of the beam and the current fraction were determined for each type of fragmentation. A TOF mass spectrometry system that significantly improved the signal-to-noise ratio was built. Using this system, the components of the thruster beam were determined. The results showed that the thruster worked in the pure ion regime. Also, the thruster delivered a maximum thrust of 67.1 μN with specific impulses of 3952 and 3117 s in the positive mode and negative mode, respectively.

ORCID iDs

Chong CHEN (陈冲) https://orcid.org/0000-0003-2092-3614

References

[1] Lozano P C, Martínez-Sánchez M and Hruby V 2010 Electrospray propulsion *Encyclopedia of Aerospace Engineering* ed K J Yoon *et al* (New York: Wiley)
[2] Rosell-Llompart J, Grifoll J and Loscertales I G 2018 *J. Aerosol Sci.* **125** 2
[3] Taylor G I 1964 *Proc. R. Soc.* A **280** 383
[4] De La Mora J F and Loscertales I G 1994 *J. Fluid Mech.* **260** 155
[5] Romero-Sanz I *et al* 2003 *J. Appl. Phys.* **94** 3599
[6] Lozano P 2003 Studies on the ion-droplet mixed regime in colloid thrusters *PhD Thesis* Massachusetts Institute of Technology, Cambridge, USA
[7] Krpoun R and Shea H 2008 Onset voltage modeling of micromachined colloid thrusters *Proc. 44th AIAA/ASME/SAE/ASEE Joint Propulsion Conf. & Exhibit (Hartford, CT, USA)* (Reston, VA: AIAA)
[8] Tajmar M, Genovese A and Steiger W 2004 *J. Propul. Power* **20** 211
[9] Paita L *et al* 2009 Alta's FT-150 FEEP microthruster: development and qualification status *Proc. 31st Int. Electric Propulsion Conf. (Michigan, USA 2009)* (IEPC)
[10] Ziemer J *et al* 2017 Colloid microthruster flight performance results from space technology 7 disturbance reduction system *Proc. 35th Int. Electric Propulsion Conf. (Atlanta, GA, USA, 2017)* (NASA Headquarters)
[11] Lenguito G and Gomez A 2014 *J. Microelectromech. Syst.* **23** 689
[12] Krpoun R *et al* 2009 *Appl. Phys. Lett.* **94** 163502
[13] Dandavino S *et al* 2014 *J. Micromech. Microeng.* **24** 075011
[14] Inoue N *et al* 2019 *Japan. J. Appl. Phys.* **58** SEEG04
[15] Gassend B *et al* 2009 *J. Microelectromech. Syst.* **18** 679
[16] Hill F A *et al* 2014 *J. Microelectromech. Syst.* **23** 1237
[17] Courtney D G, Li H Q and Lozano P 2012 *J. Phys. D: Appl. Phys.* **45** 485203
[18] Krejci D *et al* 2017 *J. Spacecr. Rockets* **54** 447
[19] Liu X Y *et al Rev. Sci. Instrum.* **90** 123304
[20] Ma C, Bull T and Ryan C 2017 Feasibility study of a micro-electrospray thruster based on a porous glass emitter substrate *Proc. 35th Int. Electric Propulsion Conf. (Atlanta, Georgia, USA, 2017)* (IEPC)
[21] Courtney D G, Dandavino S and Shea H 2016 *J. Propul. Power* **32** 392
[22] Krejci D and Lozano P 2017 Micro-machined ionic liquid electrospray thrusters for Cubesat applications *Proc. 35th Int. Electric Propulsion Conf. (Atlanta, Georgia, USA, 2017)* (IEPC)
[23] Biagioni L *et al* 2005 Qualification status of the FEEP-150 electric micropropulsion subsystem *Proc. 41st AIAA/ASME/SAE/ASEE Joint Propulsion Conf. & Exhibit (Tucson, Arizona, USA, 2005)* (Reston, VA: AIAA)
[24] Lenguito G, de la Mora J F and Gomez A 2014 *J. Micromech. Microeng.* **24** 055003
[25] Fridman A and Kennedy L A 2011 *Plasma Physics and Engineering* 2nd edn (Boca Raton, FL: CRC Press)
[26] Iribarne J V and Thomson B A 1976 *J. Chem. Phys.* **64** 2287
[27] Miller C E and Lozano P C 2016 Measurement of the fragmentation rates of solvated ions in ion electrospray thrusters *Proc. 52nd AIAA/SAE/ASEE Joint Propulsion Conf. (Salt Lake City, UT, USA)* (Reston, VA: AIAA)
[28] Gamero-Castano M and Hruby V 2011 *J. Propul. Power* **17** 977